*Mechanical Systems and Signal Processing* (2003) **17**(2), 285–303
doi:10.1006/mssp.2001.1425, available online at http://www.idealibrary.com on IDEAL®

# STRUCTURAL HEALTH MONITORING OF AN AIRCRAFT JOINT

T. Mickens, M. Schulz, M. Sundaresan and A. Ghoshal

*Intelligent Structures and Mechanisms Laboratory, Department of Mechanical Engineering, North Carolina A&T State University, Greensboro, NC 27411, U.S.A. E-mail: schulz@ncat.edu*

A. S. Naser

*Lockheed Martin, C/O NASA Langley Research Center, Mail Stop 303, Hampton, VA 23681-0001, U.S.A.*

AND

R. Reichmeider

*National Instruments, Raleigh, NC 27609, U.S.A.*

*(Received 10 July 2000, accepted 1 April 2001)*

A major concern with ageing aircraft is the deterioration of structural components in the form of fatigue cracks at fastener holes, loose rivets and debonding of joints. These faults in conjunction with corrosion can lead to multiple-site damage and pose a hazard to flight. Developing a simple vibration-based method of damage detection for monitoring ageing structures is considered in this paper. The method is intended to detect damage during operation of the vehicle before the damage can propagate and cause catastrophic failure of aircraft components. It is typical that only a limited number of sensors could be used on the structure and damage can occur anywhere on the surface or inside the structure. The research performed was to investigate use of the chirp vibration responses of an aircraft wing tip to detect, locate and approximately quantify damage. The technique uses four piezoelectric patches alternatively as actuators and sensors to send and receive vibration diagnostic signals. Loosening of selected screws simulated damage to the wing tip. The results obtained from the testing led to the concept of a sensor tape to detect damage at joints in an aircraft structure.



## 1. INTRODUCTION

Damage detection has become a key research area in the field of mechanical and aerospace engineering. In the past decade, methods for identifying damage have been intensively investigated [1–12]. Increasing safety and reliability, and extending the life of structures by adopting conditioned-based maintenance strategies is the driving force behind structural health monitoring (SHM) methods. SHM generally implies using an *in-situ* monitoring system to detect damage, whereas conventional non-destructive evaluation (NDE) inspections are done at periodic maintenance checks. SHM is important because many structures are being used beyond their design lifetimes, and the integrity of the structure must be monitored during operation to prevent failure. Also, future structures such as reusable launch vehicles are being designed with integrated Health Management Systems to reduce maintenance costs and improve safety. Monitoring the condition of a structure during its operation to diagnose any faults as they occur can provide the advantages of lighter, faster,

0888–3270/03/ + $30.00/0 

cheaper, safer, longer lasting and more reliable structures. Monitoring requires placing some type of sensor system on the structure to measure a physical quantity such as vibration, strain, thermal emissions, acoustic emissions, chemical species or electrical conductivity. Measurements from the sensor system are interpreted to provide information on five possible levels of condition diagnosis; (1) damage detection, (2) damage location, (3) damage magnitude, (4) condition-based performance, and (5) predicting the remaining life of the structure. The applications for this technology when matured are enormous, encompassing aerospace, ageing aircraft, high-speed civil transport aircraft, reusable launch vehicles, space vehicles, armoured vehicles, ships, civil infrastructure, wind turbines and others. While there are many possible applications, in-operation inspection or operational health monitoring is much more challenging than ground inspection or stationary inspection, and conventional NDE methods may not be suitable for SHM. There is also a need to develop special SHM techniques and sensors for structures that are inaccessible due to their large or small size or they require disassembly, or they are in motion such as rotating systems, or they operate in a hazardous environment or at high temperatures.

In this paper, smart materials are employed for damage detection because of their sensitivity and reliability. These materials will send vibration or waves through a structure and propagation of the vibration or waves will be measured to monitor the structure for damage. Damage sites will cause changes in the magnitude and phase of vibration or changes in the reflection and diffraction of waves, and these changes will allow identification of damage. The design of the *in-situ* sensor system is the most important and challenging aspect of designing a health monitoring system. To optimise the sensor system design, different frequency ranges of operation and sensor configurations must be investigated. Smart materials that can be used as sensors to measure vibration and wave propagation include lead zirconate titanate (PZT) monolithic wafers, interdigitated (IDT) PZT monolithic wafers, polyvinylidene fluoride (PVDF) films and piezoceramic active fibre composite (AFC) materials. Fibre optic wires, smart paint, strain gauges and accelerometers can also be used for operational health monitoring.

Each type of sensor has advantages for specific applications. Strain gauges are accurate but give a localised measurement. Acoustic emission sensors detect propagation of a crack, but do not sense damage unless it is propagating, and they are sensitive to noise in the measurement. Fibre-optic wires can sense strain and vibration, but are difficult to fit to structures that have complex geometry and the measurement is very localised. Piezoceramic materials can detect damage using vibration frequency response function(s) (FRF)s or waves or other signal processing methods. Guidelines and design algorithms for the use of different sensor types need to be developed, and simulation and testing must be performed to verify the techniques. The simplest algorithms that detect damage using vibration measurements will compare the healthy and after damage signals in the relatively higher frequency ranges to detect and locate damage. Damage indicators can be based on the magnitudes or the integrated differences in the magnitudes of the signals. Damage can be detected using FRFs, but the frequency domain methods are often overly sensitive to the normal structural condition [1–4]. To make the vibration-based method practical, the measured FRFs of the operational structure must be compensated for changes in the structure due to the environment. These changes can be modelled as changes in overall stiffness of the structure. A method of damage detection and localisation in rivet lines in a section of a metallic wing tip structure is investigated in this paper.

## 2. DAMAGE DETECTION USING FREQUENCY RESPONSE FUNCTIONS

The dynamic properties of physical systems are usually described in terms of some linear transformation of the time response of the system. A Fourier transformation [13, 14]

produces a direct frequency-domain description of the system properties. The FRF is the Fourier transform of the response or output of the system divided by the Fourier transform of the excitation or input to the system. The physical interpretation of the FRF variable $H(f)$ is that a sinusoidal input at frequency $f$ will produce a sinusoidal output at exactly the same frequency $f$, but the amplitude of the output will generally be different from the input amplitude, and the output will generally be shifted in phase from the input. The complex FRF describes the ratio of the magnitude of the output response divided by the input, and the phase lag of the output relative to the input.

The FRF is desirable from the viewpoint of applications for SHM because structural FRFs are sensitive to small changes and damage in a structure. To quantify this sensitivity, a damage indicator was developed to quantify the difference in the FRF response between healthy and damaged structures. The damage indicator for the structure is developed considering first the percent difference between the magnitude of the FRFs of the healthy and damaged structures:

$$y(f) = abs\left(\frac{|H^h| - |H^d|}{|H^h|}\right) \tag{1}$$

where the superscripts $h$ and $d$ represent the healthy and damaged structures, respectively, and the vertical bars represent the magnitude of the function. Any physical quantity can be used to compute the FRF, examples are acceleration/force, velocity/force, displacement/force, strain/force or PZT sensor voltage/PZT excitation voltage. The damage indicator $D$ is obtained by computing the mean of $y(f)$ over the frequency range of interest. This is given as

$$D = \frac{1}{(f_2 - f_1)} \int_{f_1}^{f_2} y(f)\,\mathrm{d}f \tag{2}$$

where $f_1$ is the lower frequency, and $f_2$ is the upper frequency of the range of interest. For discrete sampling, equation (2) can be written as

$$D = \frac{\Delta f}{(f_2 - f_1)} \sum_{i}^{n} y_i(f) \tag{3}$$

where $\Delta f$ is the frequency increment between measurement points. Equations (1)–(3) provide a damage indicator that gives a normalised measure of damage found in the structure. These values once collected for different sensor/actuator pairs can roughly quantify the amount of damage in a structure. Since the FRFs of a structure are dependent on the stiffness and damping properties, the FRFs indicate changes or damage to a structure, which is demonstrated in this paper.

### 2.1. FRF CORRECTION DUE TO TEMPERATURE CHANGES

Environmental effects such as temperature or pressure changes or ageing of the structure may cause global changes in the structural properties. These global changes are not due to damage, but they also change the FRFs of the structure. A problem related to using FRFs for damage detection is that the change in FRFs due to environmental effects is difficult to separate from changes in the FRFs due to damage. For example, the effect of a temperature increase of the structure is to decrease the elastic modulus and this decreases the stiffness of the structure and shifts the FRFs to lower frequencies. The boundary conditions and in-plane forces may also be affected by temperature changes. Therefore, it is desired to improve the accuracy of using FRFs for damage detection in practical applications where there are changes in the operating environment. In this section, the temperature sensitivity

of FRFs is examined by assuming that the temperature change causes a global change in the stiffness of the structure. The effect of the temperature change is then corrected using an iterative algorithm described below.

The procedure to correct FRFs for environmental effects is developed by considering the healthy FRFs and the changed FRFs due to an overall temperature change or reduction in stiffness of the structure. If the peaks of the FRFs are well spaced, the FRFs will be dominated by one term near each resonance. If each peak in the FRF is considered as a single degree of freedom (DOF) system (sdof), then the amplitude of the FRF for DOF $r$ can be written as

$$|H_r| = \frac{1}{\lfloor (K_r - \omega_r^2 M_r)^2 + (\omega_r C_r)^2 \rfloor^{1/2}}. \tag{4}$$

Letting $C_r = 2\xi_r \omega_r M_r$ and considering the resonance condition, equation (4) becomes

$$|H_r|_{\text{resonance}} = \frac{1}{(2\xi_r M_r \omega_r^2)}. \tag{5}$$

The FRF for the changed system (the $i$ system) must be corrected for environmental effects for comparison to the FRF from the healthy system (the $j$ system). Assuming that a temperature change causes a stiffness change, and that the mass (M) and damping ratio ($\xi$) stay the same, then, using equation (5), the ratio of the FRFs for the changed system ($i$) and the healthy system ($j$) at resonance is

$$\left|\frac{H_j}{H_i}\right| = \left(\frac{\omega_i}{\omega_j}\right)^2 = \frac{K_i}{K_j}. \tag{6}$$

The stiffnesses are not known, but the stiffness of the changed structure $K_i$ can be represented as being proportional to the stiffness of the healthy structure $K_j$ as $K_i = \alpha K_j$. Then from (6)

$$|H_j| = \alpha |H_i|. \tag{7}$$

Equation (7) gives the amplitude correction for the FRF of the changed system. Once the amplitudes are corrected, the frequencies must be corrected. This can be done by substituting $K_i = \alpha K_j$ into the right-hand side of equation (6) and solving, which gives

$$\omega_j = \frac{\omega_i}{\sqrt{\alpha}}. \tag{8}$$

Therefore, the iterative algorithm works by starting with $\alpha = 1$, or no environmental change, and when change or damage is sensed, the value of $\alpha$ is adjusted by iteration and the FRFs are corrected using equations (7) and (8) to minimise the magnitude of the difference in the FRFs, which is given by the damage indicator (3). This procedure is similar to stretching or compressing horizontally and vertically the changed FRF to align to the healthy one. The correction is a function of frequency applied over the full frequency range of the analysis and the same correction is used for the FRFs at all dofs.

### 2.2. DAMAGE DETECTION SIMULATION

The damage detection technique described by equations (1)–(3) uses input–output FRFs measured on the healthy and in-service structure, but no modelling of the structure is used. A FEM model (Fig. 1) is used in this section only to test the damage detection technique and for guiding the design of the sensor system. A cantilever beam model is used for the


Figure 1. Fixed–free beam element numbers and nodal dofs for simulation.

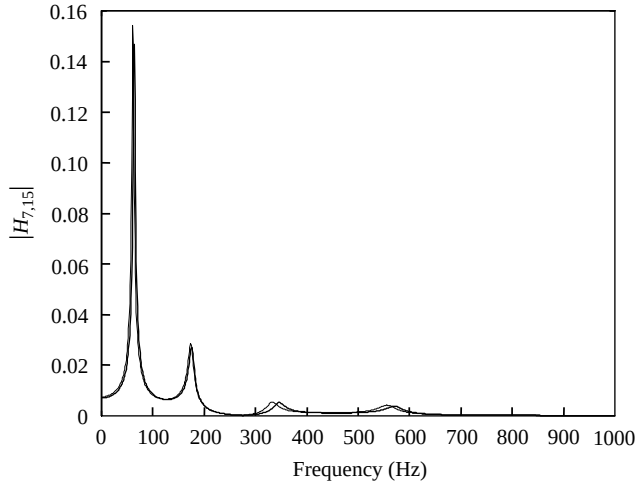


Figure 2. Simulation of healthy and damaged FRFs at dof 7 due to the excitation at dof 15: —, healthy FRF; —, damaged FRF.

simulation. The beam length = 20 in, width = 1.0 in and the depth = 0.125. The modulus of elasticity of the aluminium material is $E = 10^7$ psi, and the weight density = 0.098 lb/in$^3$.

The beam has 10 elements and 20 dofs, with a translation and rotation dof at each node. Excitation is at dof 15, and the response is at dof 7. There is 40% damage to element number five that is simulated by reducing the magnitude of all values in the elemental stiffness matrix of the damaged element. The response is computed with a frequency spacing of 1 Hz. A PC and MATLAB were used to perform the simulations. In the simulation, damping is modelled using a constant damping ratio of 0.03, and a frequency-dependent damping matrix is computed at each frequency point in the FRF computation. This approach prevents the unrealistic high damping values obtained when using the typical proportional damping approach based on two parameters, and it prevents coupling of all dof and smearing damage that occurs when using modal damping and transforming back to the physical coordinate system. The FRFs for the healthy and damaged beams are shown in Fig. 2. Using equation (3), the damage indicator value is computed as $D = 0.1942$. The seemingly large value of $D$ occurs because the damage indicator involves division of FRFs. When damage occurs to structures with small damping, the FRFs for the healthy and damaged structures misalign, and because they are functions with many peaks and valleys the small misalignments in frequency can cause large changes in their division when the damage indicator function is computed.

Next, a 4% global 'environmental change' or reduction in stiffness is put in the entire healthy beam to simulate an increase in temperature to test the correction algorithm. Here the excitation is at dof 17, and the response is at dof 5. Notice in Fig. 3(a), with $\alpha = 1$

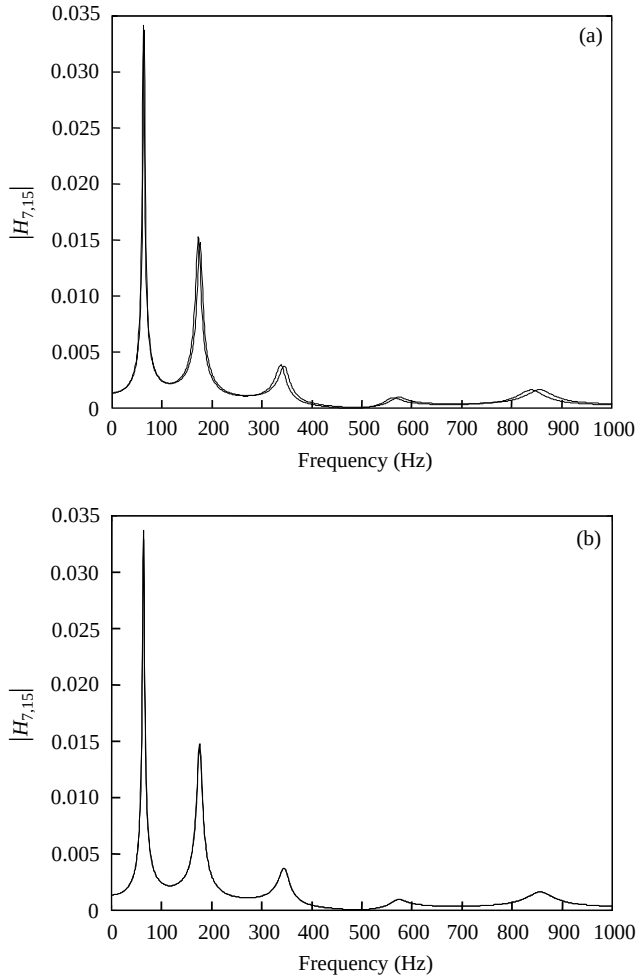


Figure 3. Simulation results for the beam finite element model, (a) FRFs healthy and changed due to an increase of temperature ($\alpha = 1$), (b) corrected and baseline FRFs ($\alpha = 0.96$): —, healthy FRF; —, adjusted FRF.

(no correction), there is a shift between the two FRFs. Then, in Fig. 3(b), applying the iteration correction due to the temperature change ($\alpha = 0.96$) results in the adjusted and healthy beam responses aligning, thus correcting for the environmental effect. The initial damage indicator value for the environmental change is $D = 0.1696$. The adjusted damage indicator value is $D = 3 \times 10^{-6}$. This procedure will not correct for localised damage, which changes the shape (resonance frequencies and amplitudes) of only part of the FRFs. Structures with spatial variations in material or temperature would require extension of the present algorithm. Further study is needed to determine as to how the change in the elastic properties of a material as a function of temperature correlates with the change in the dynamic characteristics of structures with temperature. This should be done for different materials and may allow an initial correction of SHM data based on temperature measurements. It is interesting that FRF data might also be used in reverse to determine the temperature of the structure in the local area of the sensors. Data fusion between SHM and temperature and other data might provide a more reliable assessment of the structural health and condition than one sensor type alone.

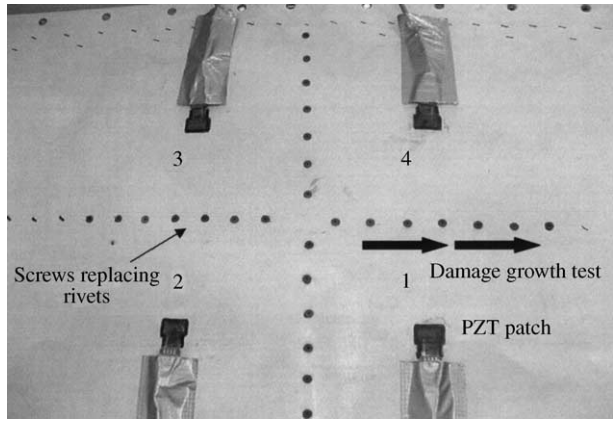


Figure 4. PZT patches bonded to the wing tip structure.

## 3. EXPERIMENTAL SET-UP

The design of a SHM system involves the integration, acquisition, analysis, visualisation and interpretation of data. The data acquisition system should eliminate aliasing and characterise the signal of interest while minimising the amount of data processing. For the experimentation performed here, four PZT patches $1/2 \times 3/8 \times 0.08$ in [15] were bonded to an airplane wing tip (Fig. 4). The patches were located approximately symmetrically from one another. A periodic chirp signal was used to excite the structure. Screws were used to replace rivets in the wing. Loosening of the screws shown in Fig. 4 simulates damage to the wing, such as corrosion or loosening at the rivets. Sensing and actuating with the PZT patches and comparing the FRFs indicates if any damage is present. By considering the symmetry of structure and PZT patches, only certain cases of excitation and damage locations will be studied. Actuating with one PZT patch and sensing with the other three can yield up to 48 different combinations of responses (by considering four patches with four different combinations of sensing/actuating and four damage locations). Since the results are similar for many cases, there was only a need to study two cases of interest. The responses for damage between PZT patches 1 and 4 will be shown, as well as the response for damage between PZT patches 2 and 3.

The data acquisition set-up used in the experimentation was controlled by a PCI-MIO-16E-1 board [16], which is a plug and play, multifunction analog, digital and timing I/O board for PCI bus computers. The board has 12- and 16-bit analog-to-digital converters, 12- and 16-bit digital-to-analog converters with voltage outputs, eight lines of TTL-compatible digital I/O, and two 24-bit counter/timers for timing I/O. Since the PCI board has no DIP switches, jumpers or potentiometers, it is easily software-configurable and calibrated. A program was written to output a chirp signal, shown in the frequency domain in Fig. 5, to one of the patches to excite the structure. A frequency range of 20–30 kHz is used because it provides the best resonant activity of the structure within the data acquisition capability of the board. After the excitation signal was output from the board it was then amplified by a 790 series power amplifier [17] by 20 times. From the amplifier, the signal was then connected to one of the four PZT patches where it actuated the wing tip while the other three PZT patches were used as sensors. The small size of the PZTs allows higher frequency vibration components to be measured. The monolithic PZT patches used are poled through the thickness and sense strain in both in-plane directions. The Signal Conditioning EXtensions for Instrumentation (SCXI) 1000 terminal box that the signals are

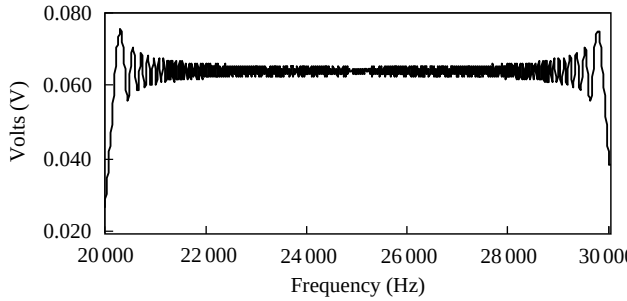


Figure 5. Excitation chirp signal at 20–30 kHz shown in the frequency domain.

routed to is called a chassis, and is able to house SCXI modules, supply power and control the data lines of the SCXI bus. The SCXI chassis is an SCXI-1141 module that can be used for anti-aliasing applications, as well as for general-purpose amplification and filtering of signals. Each one of its channels has an output range of $+5$ V and has an input amplifier with gains of 1–100. Each amplifier gain can be independently set. The analog inputs are overcharge voltage protected. The filters are low-pass, sharp roll-off, eighth-order elliptic filters that can have a cut-off frequency from 10 Hz to 25 kHz. All eight filters have the same cut-off frequency but none of these were used in the actual experimentation in order to allow the higher frequency range of analysis up to 40 kHz. Software Version 5.1 [16] was employed in conjunction with the data acquisition set-up to provide a convenient and automated data acquisition system.

A chirp signal is used to drive one of the PZT patches because it has distinct advantages in identifying closely spaced natural frequencies. The chirp is an impulsive type of input or fast sine sweep that can have excitation over a wide range of frequencies. This is important because different damages can affect different frequency ranges of a structure, and the resonant and antiresonant characteristics of a structure are good indicators of damage. This approach of using chirp vibration is a more global indicator of damage compared to methods that use single frequency tone bursts and wave reflection to detect damage. The FRFs can indicate damage that is inside the structure, whereas they may not be as sensitive to small damage on the surface as compared to wave propagation methods. The lower ($f_1$) and upper ($f_2$) frequencies that act over the chirp's time period, $T_c$, are specified to generate this input. The chirp is generated by the function:

$$v(t) = A \sin[2\pi(f_1 + \mu t/2)t + \delta] \tag{9}$$

where $v$ is the voltage, $t$ is the time, $A$ is the amplitude, $\delta$ is the arbitrary phase angle, and $\mu$ is defined by

$$\mu = \frac{f_2 - f_1}{T_c}. \tag{10}$$

To have achieved minimum filter leakage requires that the signal start and end with the same value slope that is either negative or positive. The practice of using rising–falling chirps (i.e. those that sweep up and down in frequency) and rapid sine sweeps for vibration testing is widespread. Chirps allow energy to be input to a structure over a controlled frequency band without the large deviations from the mean associated with the use of random excitation. In addition, the excitation power spectrum is fairly flat over the frequency band and the response clearly shows the structural resonant frequencies. It was

preferred to sample at a fairly high rate to achieve a good resolution for our signals of interest. A sample rate of 102 400 Hz was selected and a total of 10 240 samples were collected. This gave a resolution ($\Delta f$) of 10 Hz excitation for a frequency range of 20–30 kHz. After the data is collected, it is saved to a file where analysis of the data was performed using signal processing software [18].

## 4. DAMAGE DETECTION EXPERIMENTATION

The goal of the experimentation is to determine the optimal parameters for damage detection in the wing section. This involves testing different combinations of locations for the excitation, sensors and damage. The peaks of the measured FRFs contain significant system information in terms of natural frequencies, damping and damage. As the frequency increases, the FRF response becomes more dependent on the structure in the neighbourhood of the sensor and actuators. The actuator spacing and frequency range selected for this experiment provide a good signal level and are within the signal processing capability of the instrumentation. A different sensor spacing and different frequency range of testing would produce a different sensitivity to damage. In the experiment, the FRFs for the healthy and damaged structures are computed and compared. The algorithm given by equations (1)–(3) is used to quantify the magnitude of the damage. Various different cases of damage and sensor locations are considered with reference to the test article shown in Fig. 4. First, in Section 4.1, a repeatability analysis is performed for healthy cases in which screws are loosened and re-tightened and the damage indicator recalculated. Next, in Section 4.2, cases 1–6 show the healthy and damaged FRFs for different combinations of damage and sensor locations. Finally, in Section 4.3, a set of experiments listed as cases 7–9 is performed in which screws are progressively loosened to represent propagating damage.

### 4.1. REPEATABILITY TESTING

The damage indicator repeatability analysis is performed first. Life management of ageing aircraft is based on damage tolerances and this requires information on the detection limits of structural health monitoring techniques. A level of resolution for the healthy case was computed by taking a second collection of samples and comparing these to the initial healthy data. This case will be called the repeatable healthy case. The FRFs for all cases are very repeatable, but not being able to exactly tighten the screws the same in every case caused some changes in the FRFs because there was a change in the stiffness of the wing tip. The values of the damage indicator (3) are shown in Table 1. In Table 1, the initial case is before any damage has been simulated in the wing tip. Healthy case 2 is the case after damage has been simulated between PZT 1 and 2 and the structure has been returned to the

TABLE 1

*Repeatability for the healthy cases* (*screws loosened and re-tightened*)

| Damage indicator | Case 1—no loosening | Case 2—location 1–2 | Case 3—location 2–3 | Case 4—location 3–4 |
|---|---|---|---|---|
| $D(1,2)$ | 0.0753 | 0.0294 | 0.1750 | 0.1478 |
| $D(1,3)$ | 0.1786 | 0.0439 | 0.2069 | 0.1690 |
| $D(1,4)$ | 0.1683 | 0.0349 | 0.3651 | 0.4118 |

Note that $D(a,b)$ indicates which patch is actuating ($a$) and which patch is sensing ($b$). For all cases in this table, PZT patch 1 is the actuator.

TABLE 2

*Damage sensitivities with a section of screws loose*

| Damage indicator | Damage between patches 1 and 4 | Damage between patches 1 and 2 | Damage between patches 2 and 3 | Damage between patches 3 and 4 |
|---|---|---|---|---|
| $D(1,2)$ | 0.5469 | 1.2809 | 0.5434 | 0.4550 |
| $D(1,3)$ | 0.6029 | 0.5298 | 0.4574 | 0.5167 |
| $D(1,4)$ | 1.0797 | 0.4950 | 0.4276 | 0.4719 |

healthy condition. Healthy case 3 is the case after damage has been simulated between PZT 2 and 3. Healthy case 4 is the case where damage has been simulated between PZT 3 and 4. These damage values are non-zero because the repeated loosening and tightening of the screws causes the FRFs to change. In general, the non-repeatability increases from the initial case (two samples of data without the screws loosened), to case 2 (the first location of screws loosened and tightened), then case 3 (the second location of screws loosened and tightened) and case 4 (the third location of screws loosened and tightened). This indicates that as the number of screws loosened and tightened increases, the repeatability of the experiment decreases. Also, there was some temperature variation when the different sets of data were taken, and this was not compensated for in these results. Averaging of multiple sample functions can also be used to improve repeatability of the FRFs.

### 4.2. DAMAGE DETECTION TESTING

Different cases of damage are considered next. Table 2 shows the damage indicator values for the different cases of damage tested. It can be clearly seen in Table 2 that when the damage was located between the sensor and excitation signal, it is easy to detect. For these cases, the damage indicator was calculated to be 6–18 times greater than the initial healthy cases indicated by underlined values in Table 1. These results indicate that the method proposed is reliable for detecting and approximately quantifying moderate size damage in the wing tip structure. Six different damage cases are described next and Figs 6–11 show the changes in the FRFs due to the damage.

#### *4.2.1. Case* 1: *Damage between* 1,4, *actuating* 1, *sensing at* 2

A periodic chirp in the frequency range of 20–30 kHz is input at PZT 1 and the FRF responses at PZTs 2, 3 and 4 are measured for the healthy and damaged cases. A row of screws is loosened between sensors 1–4 to represent the damage. The rivets are completely loose to simulate major damage in that area of the wing tip. In Fig. 6, a key in the upper left corner is utilised to show the piezoceramic patches where excitation (E) and sensing (S) occur on the wing tip structure. The large black line in the corner figure indicates the damage location. The difference in the two signals is obvious in Fig. 6. Thus, damage can be detected from the FRF responses due to loosening of a row of screws. There is some shifting of the frequencies and amplitude changes in the frequency response. This process was repeated for all four locations of damage. Similar results were obtained from sensor 4 when the damage was moved between PZT 1 and 2 but not shown in Fig. 6. This is due to the symmetry property of the geometry of the wing tip.

#### *4.2.2. Case* 2: *damage between* 1,4, *actuating* 1, *sensing at* 3

In Fig. 7, the sensor is moved to a different location on the structure, indicated by the key in the corner. Examination of Fig. 7 shows that there is some shifting of frequencies and

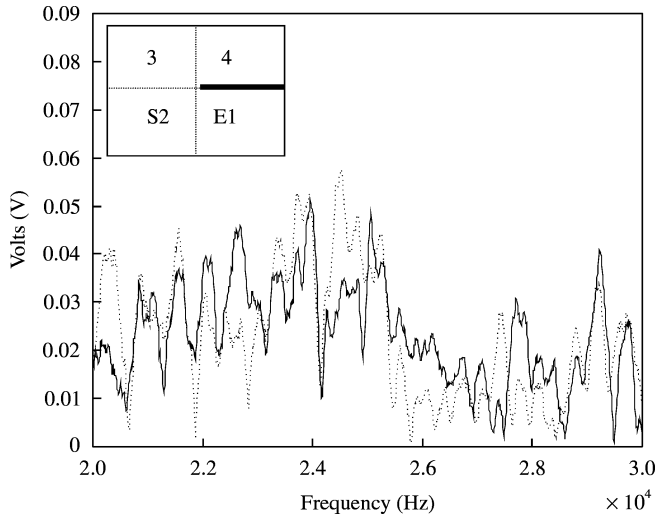


Figure 6. Healthy *vs* damaged FRFs for PZT 2, with damage between PZT 1 and 4: —, healthy; – – –, damaged.

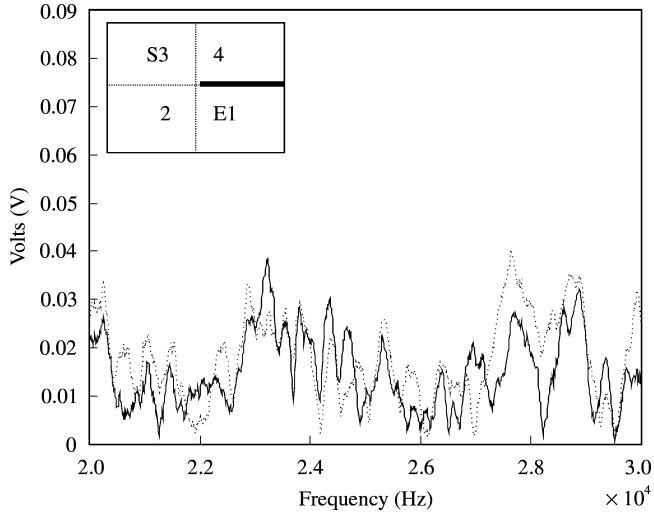


Figure 7. Healthy *vs* damaged FRFs for PZT 3, with damage between PZT 1 and 4: —, healthy; – – –, damaged.

some amplitude change, but damage is not as evident as it was in Fig. 6. From the key in the left corner, it is shown that sensing is farther from where excitation occurs, and this is mostly likely the reason for the healthy and damaged signals not differing as much as in Fig. 6. When the damage is placed between PZT 2 and 3, or between PZT 3 and 4, with PZT 1 remaining the actuator patch, similar types of responses are acquired.

### *4.2.3. Case* 3: *Damage between* 1,4, *actuating* 1, *sensing at* 4

Healthy *vs* damaged responses of the FRFs for damage between PZT 1 and 4 are shown in Fig. 8. The effect of the damage on the vibration response is very clear. In another series of

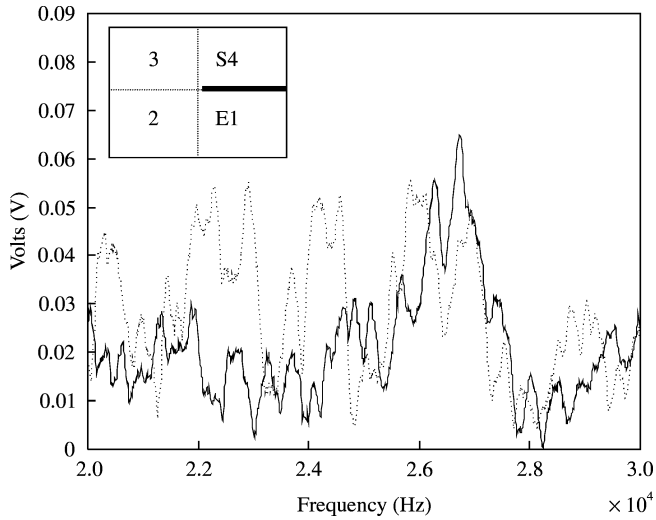


Figure 8. Healthy *vs* damaged FRFs for PZT 4, with damage between PZT 1 and 4: —, healthy; – – –, damaged.

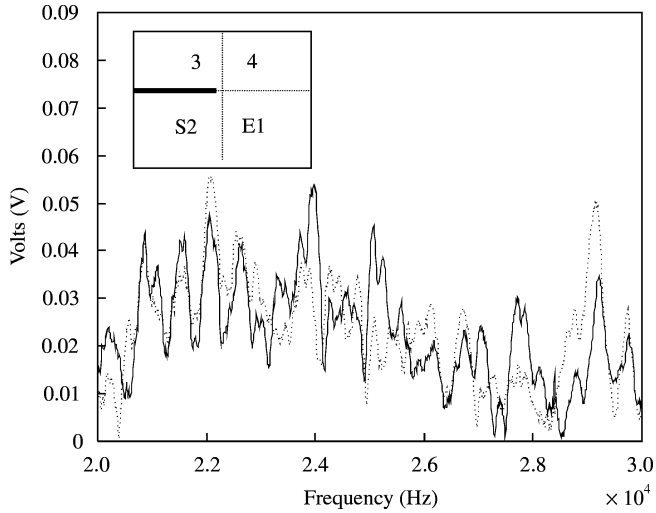


Figure 9. Healthy *vs* damaged FRFs for PZT 2, with damage between PZT 2 and 3: —, healthy; – – –, damaged.

testing not shown here [19], a periodic chirp is again input at PZT 1, but damage is moved to the location between PZT 1 and 2 with the FRF responses at PZT 2, 3 and 4 being measured for healthy and damaged cases. A general observation from the cases shown in Figs 6–8 is that the damage detection method is more sensitive when the damage is directly between the excitation and the sensor as in Fig. 8.

### *4.2.4. Case* 4: *Damage between* 2,3, *actuating* 1, *sensing at* 2

Figures 9–11 are the second location for damage in the wing tip with damage being placed between PZT 2 and 3. Based on the two locations of damage analysed thus far, a large difference in the signals is not expected. It is obvious from the earlier results that the signals tend to not differ as much if the damage is not in the direct path of the excitation

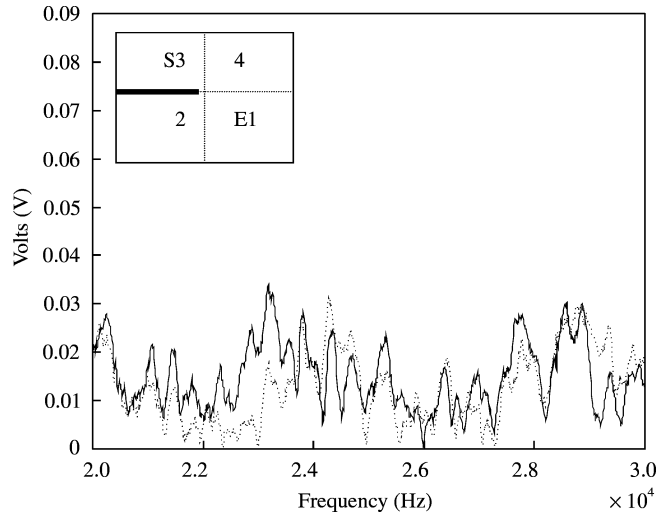


Figure 10. Healthy *vs* damaged FRFs for PZT 3, with damage between PZT 2 and 3: —, healthy; – – –, damaged.

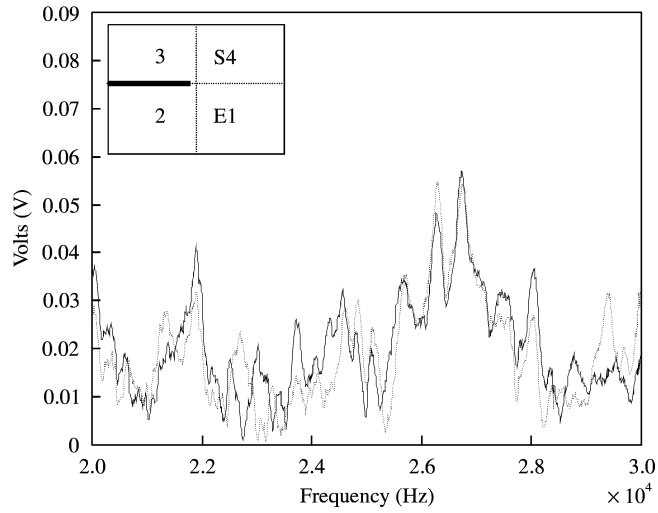


Figure 11. Healthy *vs* damaged FRFs for PZT 4, with damage between PZT 2 and 3: —, healthy; – – –, damaged.

signal. In the particular case of Fig. 9, damage is not between the sensor and actuator, and only at certain frequencies is there a noticeable change in the healthy and damaged FRFs. This makes the severity and location of the damage more difficult to determine.

*4.2.5. Case* 5: *Damage between* 2,3, *actuating* 1, *sensing at* 3

As seen in Fig. 10, the 'similarity' in the healthy and damaged signals is because the damage is not in the path of the sensor and the excitation signal.

*4.2.6. Case* 6: *Damage between* 2,3, *actuating* 1, *sensing at* 4

In this case, there are slight differences in the FRFs for the healthy *vs* damaged cases (Fig. 11), but they do not indicate damage clearly. Some shifting in the frequencies does

appear due to the change in the stiffness of the structure, but since the damage is located on the opposite side of the structure, the damage response for PZT 4 does not indicate much change.

The experiments performed show how FRFs can be used to detect damage in the wing tip and also localise the damage. The responses that are shown for Figs 6–11 show the effects of the damage clearly. For SHM, if a structure is excited at its resonant frequencies and the FRFs are calculated for two different cases, healthy *vs* damaged, these FRFs can be compared to verify the health of the structure.

### 4.3. DAMAGE SENSITIVITY TESTING

One last set of experiments will show the accuracy of the FRFs and reliability of the damage indicator together. As shown in Fig. 4, damage is simulated in the wing tip by loosening sets of screws. In this experiment, only certain screws are loosened. Starting with the centre screw between PZTs 1 and 4, this screw is loosened and then the one to the right of the centre screw, then to the left of the centre screw, and then the one next to the right are loosened. This gives a total of four loose screws for the full experiment. The experiment was run starting with one loose screw, then two screws loosened and then finally all four screws were loosened to get the third and final case of healthy *vs* damage for a simulated crack growth. From the previous section, we know that the effects of damage will be more obvious between PZT 1 and 4. As a result of this we will focus on this area to show the sensitivity. The damage values for these experiments are given in Table 3. These values confirm as to what is expected from a crack growing in a structure. As one can observe when there are four screws loose, the damage value is almost 5 times the value of the healthy case. Another trend that is noticeable is when there are two screws loose both PZT sensor signals 2 and 3 reach a maximum value and then decrease as the third screw is loosened. This occurs because loosening of the screws to simulate the crack growing in the wing tip is actually simulating a crack that is growing away from PZT 2 and 3. As in the previous cases when damage is away from the sensors, it was not detected as clearly as if it was close to the sensor or in the direct path of the sensor/actuator. The complex internal geometry and ribs in the wing tip may also have affected how the vibration propagated in the structure causing these types of results. A second case of the growing crack was performed in the section between PZT 1 and 2 to compare the effects of the two different locations. Again it was observed that the damage indicator values for $D(1,2)$ increased as the simulated crack increased in length and $D(1,3)$ and $D(1,4)$ reached a maximum with two loose screws and then decreased as the crack continued to grow. This mirrors the results in Table 3. A more in-depth study should be performed to explain this result based on mechanics principles. Comparison of the FRFs for the different numbers of screws loose is discussed in cases 7–9 below and in Figs 12–14.

TABLE 3

*Damage indicator values for increasing damage between PZT* 1 *and* 4

| Damage indicator | Healthy | 1 Screw loose | 2 Screws loose | 3 Screws loose | 4 Screws loose |
|---|---|---|---|---|---|
| $D(1,2)$ | 0.0860 | 0.3169 | 0.3201 | 0.2955 | 0.2911 |
| $D(1,3)$ | 0.2435 | 0.442 | 0.4293 | 0.3674 | 0.3713 |
| $D(1,4)$ | 0.2241 | 0.4849 | 0.5863 | 0.7966 | 1.1382 |

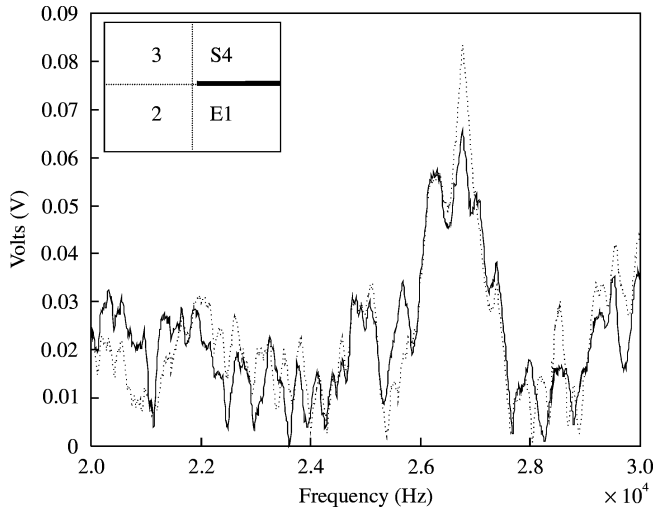


Figure 12. Healthy *vs* damaged FRFs for PZT 4. The damage is one screw loose between PZTs 1 and 4: —, healthy; – – –, 1 loose screw.

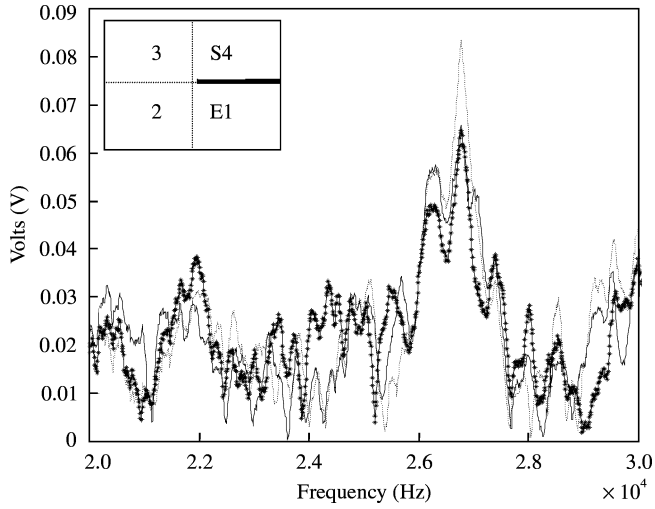


Figure 13. Healthy *vs* damaged FRFs for PZT 4. The damage is one and two screws loose between PZTs 1 and 4: —, healthy; – – –, 1 loose screw; —∗—, 2 loose screws.

*4.3.1. Case* 7: *Damage between* 1,4, *actuating* 1, *sensing at* 4, 1 *screw loose*

With only one screw loose it can be seen (Fig. 12) that the damage has a small effect when compared to the healthy signal. Some amplitude variations are noticed and one can infer that there is some damage present just from a single screw being loose.

*4.3.2. Case* 8: *Damage between* 1,4, *actuating* 1, *sensing at* 4, 1–2 *screws loose*

Figures 12 and 13 illustrate how sensitive the FRFs can be for a structure. With only two screws loose one can see how a change in the stiffness affects the structural response. In Fig. 13, the curve for the two screws loose case is significantly different from the curves of the other FRFs. This is due to the greater change in stiffness to the structure.

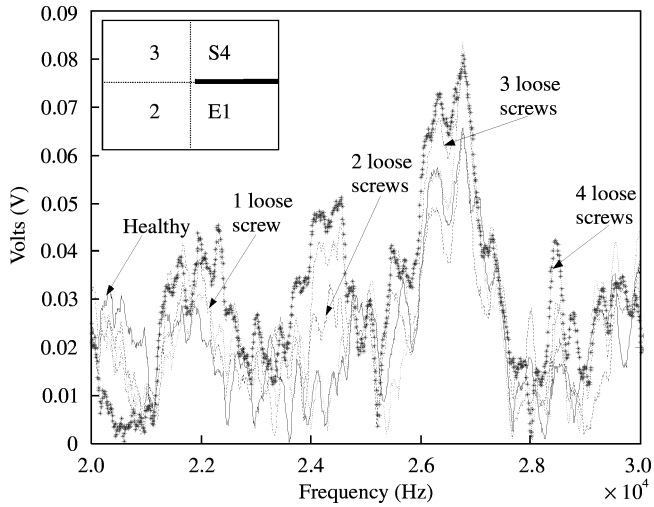


Figure 14. Healthy *vs* damaged FRFs for PZT 4. The damaged is one, two and four screws loose between PZTs 1 and 4.

*4.3.3. Case* 9: *Damage between* 1,4, *actuating* 1, *sensing at* 4, 1–4 *screws loose*

In Fig. 14, the FRFs of all the different responses are graphed together to illustrate how the increasing damage will cause the FRFs to change. Also, the three responses have different amplitudes but similar frequencies.

In cases 8 and 9, as the damage increases (the number of screws loose) the response with the greatest damage tends to envelop the other responses. Also, the damage indicator values give the severity of damage present. This SHM technique can be employed in an aircraft using historical data such as in Table 3. An operator can interpret these results as a growing fault in the area between PZT 1 and 4. This structure could then be taken from service and further testing performed using conventional NDE methods. With the use of the damage indicator, damage can not only be located, but a quantification of damage can be made. This is a simple method and algorithm that can detect defects such as loose rivets and joints and other damage. In the next section, a new sensor design is proposed. The sensor design will be useful for detecting damage in bonded or riveted joints and for the application presented here.

## 5. SENSOR TAPE FOR MONITORING STRUCTURAL JOINTS

Improved inspection techniques are needed to monitor riveted and bonded structural joints. Based on the results in this paper, it is possible that a long sensor with segments that can be multiplexed can be put on two sides of a joint and used to inspect the joint autonomously during operation of a vehicle or structure. Although there are a variety of sensors available, they may not be applicable to monitoring the condition of large continuous structures. A network of distributed reliable and economical sensors is required. Successful development and implementation of the technology for a sensor design could lead to reduction in costs associated with maintenance, minimisation of downtime, avoiding economic loss and improvement of the safe use of structures. Based on the previous considerations, and the testing performed in this paper, a sensor that can be used to detect interior damage and surface faults is proposed in Fig. 15. This sensor could be used to

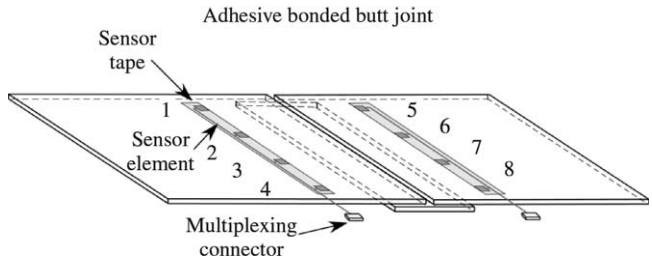


Figure 15. Sensor tape concept to detect damage at joints on a structure.

supplement conventional non-destructive testing methods. The economic saving by having a continuous inspection system in both military and commercial sectors as a whole can be significant. However, this research is ongoing and the sensor design and damage detection algorithms are being improved.

The sensor tape is constructed of PZT fibres or IDT monolithic patches in between capton sheets. The multiplexing connector is used to connect to a signal generation and data acquisition system such as a laptop PC host with data acquisition boards. The sensor operates by exciting at node 1 and sensing at node 5, exciting at node 2 and sensing at node 6 and on. This procedure can be used to continuously inspect large joints during flight by fast scanning through the actuator/sensor pairs. A minimum of computation is needed, and damage on the surface or inside the joint will change the chirp signal and will be detected. Very small cracks initiating from rivet heads could not be detected with this sensor. When the cracks begin to propagate, they can be detected.

## 6. CONCLUSIONS AND RECOMMENDATIONS

Techniques for SHM were discussed and the FRF technique was discussed in detail, including the derivation and applications. The applications presented show that the FRF monitoring method is effective and has certain advantages and limitations as compared to other SHM methods. Next, comprehensive conclusions are given and further research is suggested.

### 6.1. CONCLUSIONS

Loosening of assembled parts including rivets, bolts or glued joints is difficult to detect in aircraft and other structures. Also, flaws, voids, cracks, thin spots and other defects can be caused during manufacturing or improper assembly of parts during manufacturing, or by fatigue, impact or corrosion. It is shown that the damage indicator proposed can locate and approximate the severity of damage. When damage occurs between two sensors, the stiffness between the sensors changes and this affects the local vibration response at high frequencies. The advantages of this approach include simplicity (no need for a model), good sensitivity over a wide frequency range, capability to detect interior damage away from the sensor and low cost for implementation.

### 6.2. RECOMMENDATIONS FOR FUTURE WORK

The consistency of the experimentation can be improved by using a torque wrench to retighten all the screws after every run. Improvements in the hardware that will allow higher

frequencies to be analysed should be investigated. The next step of the research is to optimise the spacing and location of sensors on the wing tip, evaluate the effect and test the correction algorithm for environmental effects and develop methods to distinguish transducer damage from structural damage. Different structures and materials should be tested to determine how sensitive this method is. A spectrogram image should be added to improve the real-time analysis of the structure under different conditions. The use of the new sensor design proposed would greatly aid the inspection of structures, but several factors need to be addressed before field implementation is feasible. These include multiplexing the sensor segments so that a compact sensor can interrogate a long joint, use of IDT sensors and sensor size and spacing. Additionally, the sensitivity and damage localisation capability of the method is expected to increase if higher frequencies are used in the experiment.

## ACKNOWLEDGEMENT

This material is based upon work supported by the NASA Marshall Space Flight Center under grant number NAG8-1646, and by the National Renewable Energy Laboratory under grant XCX-7-16469-01. The wing tip was donated for the experiment by Tradewinds Airlines of Greensboro, NC. This support is gratefully acknowledged.

## REFERENCES

1. H. ZHANG, M. J. SCHULZ, A. S. NASER, F. FERGUSON and P. F. PAI 1999 *Mechanical Systems and Signal Processing* **13**, 765–787. Structural health monitoring using transmittance functions.
2. M. J. SCHULZ, P. F. PAI, A. S. NASER, S. K. THYAGARAJAN, G. R. BRANNON and J. CHUNG 1997 In *Locating Structural Damage Using Frequency Response Reference Functions and Curvatures.* Fu-Kuo Chang (ed.). Lancaster, PA: *Technomic Publishing Company, Inc.*
3. M. J. SCHULZ, P. F. PAI and A. S. NASER 1996 *IMAC-XIV Conference, February 12–15, Dearborn, MI.* Frequency response function assignment technique for structural damage identification.
4. S. K. THYAGARAJAN, M. J. SCHULZ, P. F. PAI and J. CHUNG 1998 *Journal of Sound and Vibration* **210**, 162–170. Detecting Structural Damage using Frequency Response Functions [letter to the editor].
5. J. N. KUDVA *et al.* 1993 *SPIE Smart Structures Conference, Alburquerque, NM.* Smart structures concepts for aircraft structural health monitoring.
6. F. K. CHANG 1997 *A summary Report on the First Stanford Workshop on Structural Health Monitoring*, September 18–20. Structural health monitoring.
7. W. N. MARTIN, M. J. SCHULZ, A. S. NASER, P. F. PAI and C. WILKERSON 1999 *5th International Conference on Composites Engineering*, 597–598, *Las Vegas, NV, July 5–11.* Detecting damage on symmetric structures using vibration measurements.
8. F. BRANCALEONI, D. SPINA and C. VALENTE 1993 *Vieweg International Scientific Book Series, Braunshwieg/Wiesbaden, Germany.* Damage assessment from the dynamic response of deteriorating structures.
9. S. W. DOEBLING, C. FARRAR, M. B. PRIME and D. W. SHEVITZ 1996 *Los Alamos National Laboratory Report LA-13070-VA5.* Damage identification and health monitoring of structural and mechanical systems from changes in their vibration characteristics: a literature review.
10. F. CHANG 1997 *The Proceedings of Structural Health Monitoring: Current Status and Perspectives Stanford University, Stanford, CA* (edited) September 18–20.
11. M. A. MANNAN and M. H. RICHARDSON 1990 *IMAC VIII, January.* Detection and location of structural cracks using FRF measurements.
12. P. MOORE, S. NESS and P. MCINTIRE 1999 *Nondestructive Testing Handbook, Vol. 10, 2nd edn. Book News, Inc., Portland Oregon.* Nondestructive testing overview.

13. K. G. CONNELL 1995 *Vibration Testing: Theory and Practice*. New York: Wiley-Interscience.
14. P. H. WIRSCHING, T. L. PAEZ and K. ORITZ 1995 New York: *Random Vibrations: Theory and Practice*. Wiley-Interscience.
15. ACTIVE CONTROL EXPERTS, MA.
16. *LABVIEW Users Guide*. TX: National Instruments.
17. PCB PIEZOTRONICS INC., Depew, NY.
18. *MATLAB Users Guide*. Natick, MA: Mathworks. Inc.
19. T. D. MICKENS 2000 MS thesis, North Carolina A&T State University, Greensboro, NC. Structural health monitoring of a wing tip.